



Power Electronic Systems
Laboratory

© 2021 IEEE

Proceedings of the 24th International Conference on Electrical Machines and Systems (ICEMS 2021),
Gyeongju, Korea, October 31-November 3, 2021

Concept of a Novel Bearingless Three-Pole Motor for Two-Sided Driven Applications

I. Bagaric,
D. Steinert,
T. Nussbaumer,
J. W. Kolar

Personal use of this material is permitted. Permission from IEEE must be obtained for all other uses, in any current or future media, including reprinting/republishing this material for advertising or promotional purposes, creating new collective works, for resale or redistribution to servers or lists, or reuse of any copyrighted component of this work in other works.



Eidgenössische Technische Hochschule Zürich
Swiss Federal Institute of Technology Zurich

Concept of a Novel Bearingless Three-Pole Motor for Two-Sided Driven Applications

Ivana Bagaric*, Daniel Steinert†, Thomas Nussbaumer† and Johann W. Kolar*

*Power Electronic Systems Laboratory, ETH Zurich, Switzerland, bagaric@lem.ee.ethz.ch

†Levitronix GmbH, Zurich, Switzerland, steinert@levitronix.com

Abstract—This paper presents a novel bearingless three-pole motor for two-sided driven applications, i. e., two motors levitating and rotating a common rotor without any mechanical contact. When operating in chemically demanding environments its advantages are highly promising: the bearingless technology allows friction- and wear-free motion, unlimited lifetime and a hermetically sealed encapsulation of the rotor, while the novel motor convinces with its - in terms of hardware - minimalistic, compact and safe design. Using 3D FEM simulations, the new topology is evaluated focusing on maximal torque and sufficient bearing forces while satisfying the compactness requirements.

Index Terms—magnetic levitation, bearingless motors, 3D-FEM, cross-flow fan

I. INTRODUCTION

By means of magnetic fields, bearingless motors levitate and spin rotors without any mechanical contact while integrating the bearing and drive functionality in one compact unit. This friction- and wear-free technology enriches many demanding applications in the semiconductor, pharmaceutical or biomedical industry such as pumps [1], mixers [2] or fans [3]. The various bearingless systems convince with their long lifetime, low maintenance costs and a hermetically sealed encapsulation of the rotor enabling implementations in the harshest of environments. These so-called bearingless *slice* motors are characterized by their much smaller stator and rotor lengths compared to their rotor diameters ($L < d/2$). Attracting reluctance forces between stator iron and rotor magnets act in favor of axial and tilting stability. In order to control the remaining three degrees of freedom, the rotational degree of freedom (DOF) and two radial DOFs have to be actively stabilized by appropriate control currents. It holds that the force-current and torque-current relations depend on the angular rotor position. To cover the whole angular range and thereby enabling full motor performance, the selection of stator teeth and rotor pole pair number is a crucial step.

The novel challenge tackled by this work is to achieve a stable levitation and rotation of long shafts ($L_{\text{shaft}} \gg d_{\text{shaft}}$) by bearingless motors. A possible industry application could include a double-sided driven cross-flow fan for gas circulation systems in excimer laser [4]. A previously introduced, fully operational bearingless six-pole motor, i.e., the stator has six teeth and six corresponding coils, is shown in Fig. 1a [5]. The commissioning of a cross-flow fan has been successful and is described in [5] as well. It requires two motors to levitate and rotate the common shaft.

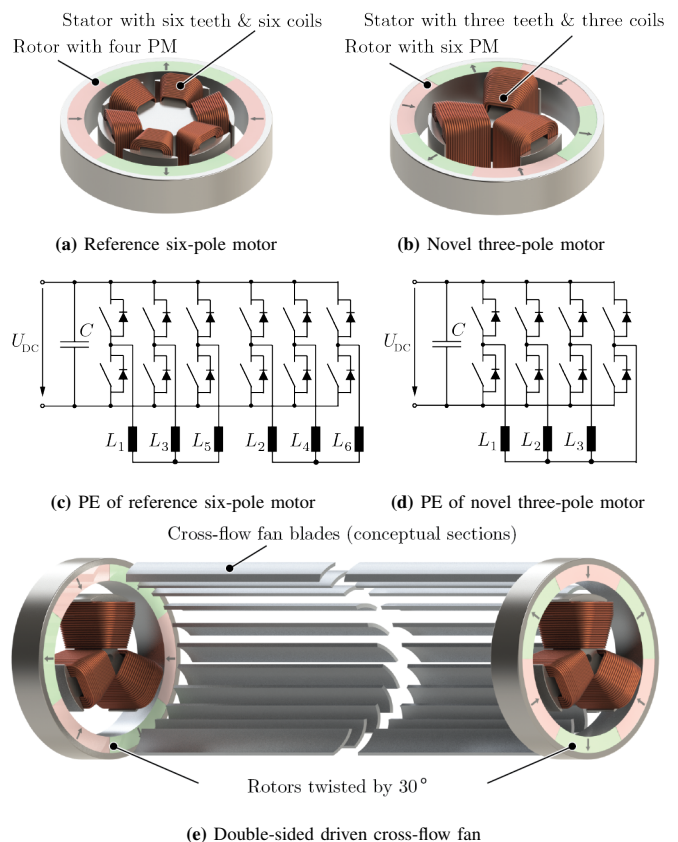


Fig. 1: Conceptual drawing of (a) the six-pole reference motor, (b) the novel, highly compact three-pole motor, (c) the power electronics (PE) of the six-pole reference motor, where 6 half-bridges are required to control the six coil currents, (d) the reduced PE of the novel three-pole motor, where only four half-bridges are necessary and (e) the bearingless cross-flow fan driven by two 30° shifted bearingless three-pole motors as an exemplary application.

The goal of this paper is to introduce the novel three-pole motor topology for two-sided driven applications (cf. Fig. 1b). Reducing the stator topology from six to three teeth leads to an elegantly compact, simple design featuring lower material and manufacturing costs as well as simplified power electronics (from Fig. 1c to Fig. 1d). However, the three-pole motor experiences single-phase drive characteristics, which has to be taken into account carefully for double-sided driven applications. The focus of this work lies on solving the single-phase drive deficit and designing an optimal motor geometry such that maximal drive torque and sufficient bearing forces

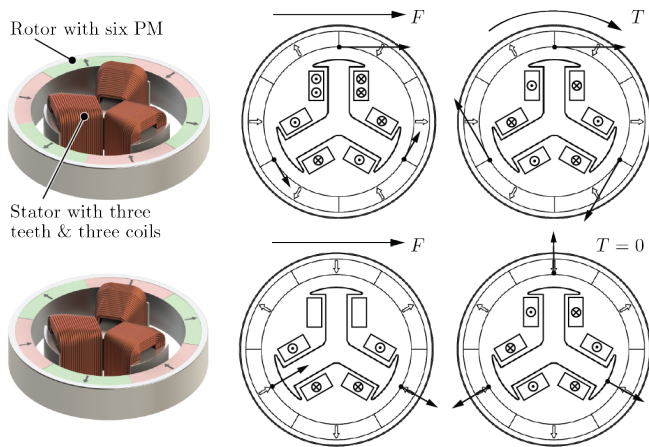


Fig. 2: Conceptual drawing of the proposed three-pole bearingless motor. The rotor consists of six permanent magnets (PM) that are magnetized in alternating order. The sketches demonstrate its force and torque generation.

are delivered from this highly compact entity. The drive torque behavior of a single as well as coupled motor is analyzed by means of 3D magnetostatic simulations in **Sec. III**. Similarly, **Sec. IV** evaluates its potential of generating active magnetic bearing forces. The influence of stator geometry parameters on the force-torque behavior is embedded in these sections as well. Finally, motor losses are studied in **Sec. V**.

II. THE THREE-POLE BEARINGLESS MOTOR

This paper aims to introduce a particularly compact and minimalistic novel motor topology. To minimize the motor's dimensions and maximize its power density compared to bearingless motors with separated windings, it is necessary to drastically reduce the number of stator teeth. **Fig. 2** illustrates the proposed topology where three coils (with combined bearing and drive functionality) are each wound onto one of the three stator teeth, representing the most compact configuration possible.

A. Passive Bearing

For bearingless slice (or disc-type) motors axial and tilting deflections are passively stabilized. When dislocating the rotor in axial z -direction or tilting it around the x - or y -axis, reluctance forces counteract this movement. The extent to which they react is defined by the axial passive stiffness

$$c_z = \frac{\Delta F_z}{\Delta e_z} \quad (1)$$

and two tilting stiffnesses

$$c_\alpha = \frac{\Delta T_\alpha}{\Delta \alpha} \quad \text{and} \quad c_\beta = \frac{\Delta T_\beta}{\Delta \beta}. \quad (2)$$

Using the possibility of passive stabilization contributes to designing a highly compact mechatronical system, however, it is physically impossible to stabilize all DOF's purely passively (Earnshaw's theorem [6]).

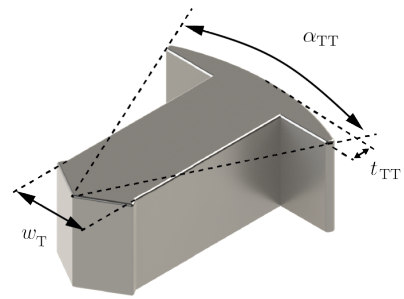


Fig. 3: Single stator tooth of the three-pole motor with its main geometry parameters, i.e., tooth width w_T , tooth tip opening angle α_{TT} and tooth tip thickness t_{TT} .

B. Active Bearing and Drive

When the rotor is displaced from its center position in radial direction, resulting reluctance forces support this movement until mechanical collision occurs. This destabilizing behavior is described by the radial stiffness factors in x - and y -direction

$$c_x = \frac{\Delta F_x}{\Delta x} \quad \text{and} \quad c_y = \frac{\Delta F_y}{\Delta y}. \quad (3)$$

The purpose of the active magnetic bearing is to compensate the passive radial bearing stiffness and thereby making rotor levitation possible. The last DOF is the drive torque, which is created by a suitable harmonic wave that generates tangential forces. The harmonic wave is coming from the winding scheme in combination with harmonics from the stator teeth [7]. For the proposed three-pole motor, **Fig. 2** demonstrates the radial force and torque generation visually. As shown, a bearing force can be arbitrarily created for every rotor angle, i.e., the two radial DOFs are fully stabilized. However, for a certain rotor angle the resulting torque is zero, hence the rotational DOF has not full range.

The necessary power electronics for the active bearing and drive control is depicted in **Fig. 1d**. Each of the three coils has to be connected to a half-bridge, while the other ends should be connected in star. A fourth half-bridge is required to control the star point, since a symmetric star connection is not possible with this design. Employing this control concept, bearing forces can be arbitrarily created for every rotor angle, while the drive experiences single-phase characteristics. For comparison, the power electronics of the reference motor is shown in **Fig. 1c**, where six half-bridges are required to control the coil currents [5]. It can clearly be seen, that besides the minimalistic stator design of the three-pole motor, the expense for the power electronics is reduced as well.

C. Coupling two three-pole motors

This work investigates the challenge of levitating and rotating long shafts by the most compact bearingless motor possible. Therefore, the single-phase drive deficit of the three-pole motor has to be solved. This is realized by a 30° twist between the two motors, which ensures that at no time both motors are in the no-torque position simultaneously. It is demonstrated in **Fig. 1e** for a cross-flow fan as an example.

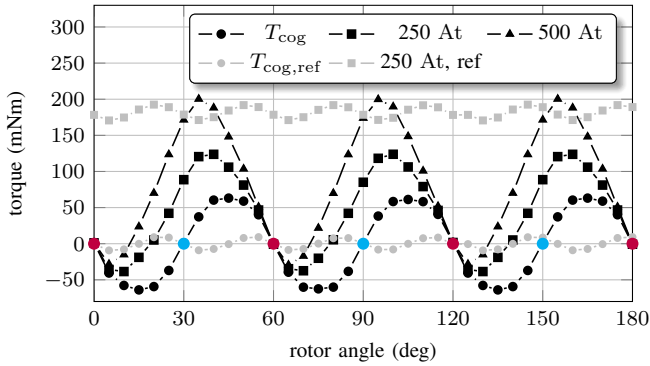


Fig. 4: Cogging torque and active drive torque with respect to rotor angle of the novel bearingless three-pole motor for excitations of $\hat{\Theta} = 0$ At (corresponding to the cogging torque T_{cog}), $\hat{\Theta} = 250$ At and $\hat{\Theta} = 500$ At. At the points marked in red, a drive torque cannot be generated. The blue points represent the unstable working points. Additionally, the cogging torque and drive torque for $\hat{\Theta} = 250$ At of the reference motor are plotted in grey.

D. Reference motor

An already existing, fully operational bearingless motor will serve as a reference, which has been presented in [5] in great detail. It consists of six stator teeth, six corresponding copper coils and a rotor with four permanent magnets as visualized in **Fig. 1a**. This comparison serves to realistically investigate the novel three-pole motor's potential and to increase the success rate of a future prototype. The reference motor's specific bearing and drive parameters, derived from 3D magnetostatic FEM simulations, are listed in **Tab. I**. For the sake of proper comparison between the reference and novel three-pole motors, some general geometry parameters have to be set as framework conditions. Therefore, the stator and rotor diameters, stator and rotor heights as well as magnet shapes of the proposed motor are set equal to the reference motor.

Using 3D magnetostatic FEM simulations the force-torque behavior of the proposed single as well as coupled three-pole motor will be evaluated next for various stator tooth geometries. Particularly, the influence of different tooth widths w_T , tooth tip opening angles α_{TT} and tooth tip thicknesses t_{TT} , as depicted in **Fig. 3**, will be studied. The focus lies on delivering maximal torque, reducing cogging torque and generating sufficient bearing forces.

TABLE I: Bearing and drive characteristics of the reference six-pole motor.

| Parameter | | | |
|-------------------------------------|--------------------|------|---------|
| drive torque constant | k_{drv} | 0.71 | mNm/A |
| bearing force constant | k_{bng} | 35.3 | mN/A |
| radial stiffness | $c_{x,y}$ | 12.2 | N/mm |
| tilting stiffness | $c_{\alpha,\beta}$ | 3.2 | mNm/deg |
| axial stiffness | c_z | 3.2 | N/mm |
| drive ripple factor for 250 A-turns | γ | 4.9 | % |

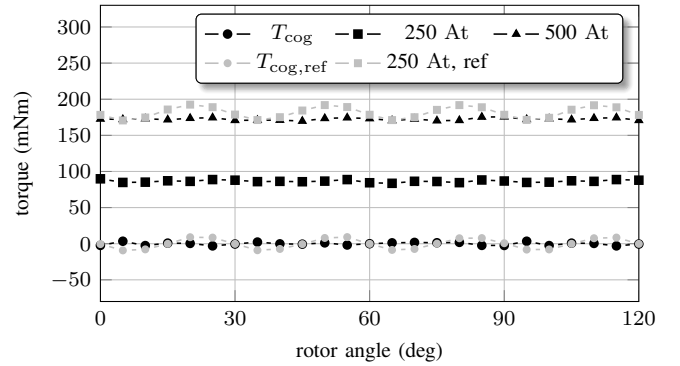


Fig. 5: Cogging torque and drive torque with respect to rotor angle of two coupled, 30° shifted novel bearingless three-pole motors, including excitations of $\hat{\Theta} = 0$ At (corresponding to the cogging torque T_{cog}), $\hat{\Theta} = 250$ At and $\hat{\Theta} = 500$ At. The no-torque positions are overcome. Additionally, the cogging torque and drive torque for $\hat{\Theta} = 250$ At of the reference motor are plotted in grey.

III. DRIVE

This section analyzes the motor's ability to generate drive torque as well as the topology's cogging torque for different rotor angles. As a first step, the behavior of a single three-pole motor is evaluated from 3D FEM simulations. From this analysis **Fig. 4** results, which shows the torque for different levels of electrical excitation. The electrical excitation (or magnetomotive force) is represented in ampere-turns (At), since it is the product of applied current and number of windings of a coil. Additionally, simulation results of the reference motor from **Tab. I** are plotted in grey for visual comparison. From **Fig. 4**, different conclusions about the three-pole motor can be drawn. This motor design produces a cogging torque, which will interfere with the active drive torque. The rotor positions marked in red represent stable points in terms of cogging torque. However, these positions coincide with the angles where active drive torque cannot be created. The rotor would stay in this position even if a drive current is applied. The positions marked in blue are unstable points, because any slight angular displacement leads to a cogging torque accelerating the rotor. In summary, this analysis confirms that the three-pole motor experiences single-phase characteristics for the drive and it would not be possible to start the rotation without special measures.

A. Coupling two three-pole motors

As described before, for double-sided driven applications the single-phase drive characteristics of the three-pole motor can be overcome by coupling them with a 30° shift. **Fig. 5** depicts the simulation results to that. The superimposed cogging torque T_{cog} shows to be much lower compared to the single three-pole motor in **Fig. 4** and angular positions where no drive torque can be generated do not exist. Comparing the effective drive torque that this setup can generate with the reference motor's torque, the simulations clearly reveal that the coupled three-pole motors create less torque than a single six-pole reference motor with the same peak magnetomotive

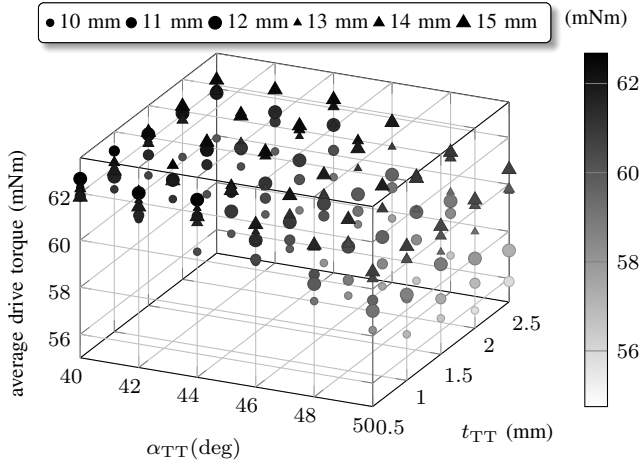


Fig. 6: Average drive torque for different stator tooth designs, i.e., varying tooth width from $w_T = 10 \dots 15$ mm, tooth tip opening angle α_{TT} and tooth tip thickness t_{TT} for $\hat{\Theta}_{drv} = 250$ At.

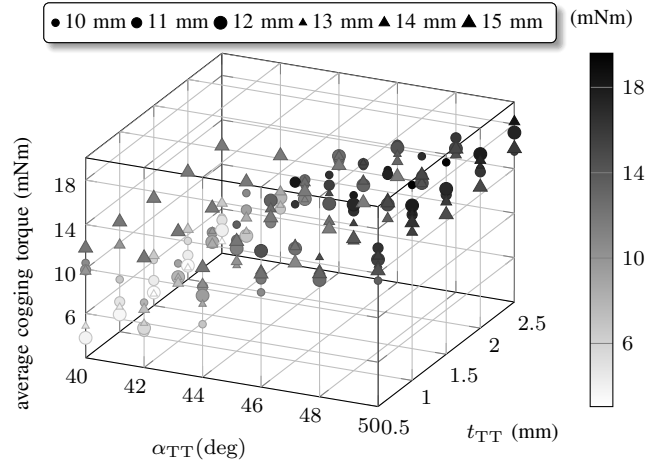


Fig. 7: Average cogging torque for different stator tooth designs, i.e., varying tooth width from $w_T = 10 \dots 15$ mm, tooth tip opening angle α_{TT} and tooth tip thickness t_{TT} .

force. This will be addressed in more detail in **Sec. V**, when looking at the motor losses.

B. Stator design and optimization

To optimize the coupled three-pole motor for high torque and low torque ripple, simulations have been conducted on the influence of stator tooth geometry (see **Fig. 3**) on the double-drive's behavior. **Fig. 6** summarizes the results of the average drive torque that is created with an electrical excitation of $\hat{\Theta}_{drv} = 250$ At (for each motor), when tooth width w_T and tooth tip form (α_{TT} and t_{TT}) are varied. Torque fluctuations over the angular range have been evaluated from these results as well. Furthermore, **Fig. 7** shows the simulation results for cogging torque with respect to the different geometry parameters. Finally, the drive ripple factor for a magnetomotive force of $\hat{\Theta}_{drv} = 250$ At is calculated from these results. After breaking all these simulation results down, different conclusions can be derived about the influence of tooth tip form and tooth width on the torque behavior.

1) *Tooth tip (α_{TT} & t_{TT}):* Interpreting **Fig. 6**, it can immediately be seen that an increase in tooth tip angle as well as thickness reduces the torque. Therefore, a design without a tooth tip acts in favor of achieving maximal torque. This can be explained by the effect of magnetic saturation. The main part of the permanent magnet flux trajectories tend to shortcut over the tip (instead of passing through the tooth itself) resulting in a torque reduction as explained in [8] in detail. Furthermore, the torque fluctuations have been evaluated. The simulations reveal that the larger the tooth tip, the stronger the fluctuations, i.e., the generated torque varies stronger with angular rotor position. Similarly, the cogging torque increases with larger tooth tip as depicted in **Fig. 7**. To get an idea on how much the cogging torque affects the drive torque, the ripple factor has been calculated according to

$$\gamma_{drv} = \frac{T_{\hat{\Theta}=0At,max}}{\bar{T}_{\hat{\Theta}=250At}} = \frac{T_{cog,max}}{\bar{T}_{\hat{\Theta}=250At}}, \quad (4)$$

with $\bar{T}_{\hat{\Theta}=250At}$ being the average torque for an electrical excitation of $\hat{\Theta}_{drv} = 250$ At and $T_{cog,max}$ the maximal cogging torque. It resulted in a γ_{drv} ranging from 4% (smallest tooth tip) up to 30% (for the largest simulated tooth tip). However, high ripple factors are not desired, since they require special measures within the control structure to ensure a smoothly running rotor. In summary, the drive simulations reveal that no tooth tip is recommended.

2) *Tooth width (w_T):* The final, crucial stator parameter is the tooth width. Choosing a small w_T prevents magnetic shortcuts, however, tends to saturation due to the small cross-sectional area which in turn has a negative influence on the resulting torque [8]. A large w_T limits the space for the copper coils and increases the chance of magnetic shortcuts [8]. To analyze these saturation effects briefly, **Fig. 8** depicts the simulation results for torque generation with respect to tooth width w_T . Tooth designs of $w_T = 6 \dots 18$ mm without a tooth tip are considered and excitation levels of $\hat{\Theta} = 0$ At, $\hat{\Theta} = 200$ At, $\hat{\Theta} = 300$ At and $\hat{\Theta} = 400$ At are applied. It results that a lower limit of w_T exists at approximately 13 mm (due to magnetic saturation) and that the cogging torque varies over the w_T range with a minimum at 13 mm.

In summary, a stator geometry is preferred, where the tooth has no tooth tip and the tooth tip has the same width as the tooth itself. This design maximizes the effective drive torque and reduces the cogging torque. Regarding the tooth width, it can be concluded that saturation effects have to be taken into account thoroughly in the stator design procedure as is also described in [8].

IV. ACTIVE MAGNETIC BEARING

After the coupled three-pole motor's drive characteristics have been studied in great detail, the bearing behavior is next. The passive reluctance forces heavily depend on the tooth geometry, since for larger stator teeth the area that the magnetic forces from the permanent magnets can act on, increases. This section will particularly focus on reluctance

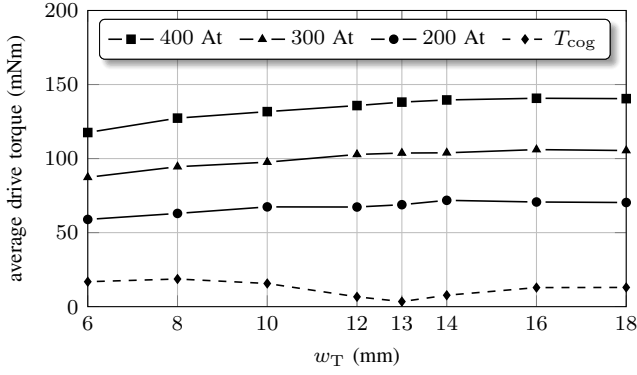


Fig. 8: Average drive torque for different tooth widths w_T and different electrical excitation levels of $\hat{\Theta} = 0$ At (corresponding to the cogging torque T_{cog}), $\hat{\Theta} = 200$ At, $\hat{\Theta} = 300$ At and $\hat{\Theta} = 400$ At.

forces for different tooth widths w_T , but excluding stator designs with tooth tips due to the explicit results from **Sec. III**. Moreover, to enable a conclusive comparison of the active magnetic bearing between the reference motor and the novel three-pole motor, the radial starting distance δ is compared. The bearing current needed to start a bearingless motor from standstill (i.e. to detach the rotor from the wall) is defined as

$$I_{start} = \frac{F_{start}}{k_{bng}} = \frac{c_{x,y} \cdot \delta}{k_{bng}} \quad (5)$$

with a required bearing force F_{start} and bearing force constant k_{bng} , whereas F_{start} is the product of the radial stiffness $c_{x,y}$ and δ . Therefore, δ is defined as

$$\delta = \frac{F_{start}}{c_{x,y}}. \quad (6)$$

Fig. 9 visualizes the simulation results for δ with respect to different tooth widths $w_T = 6 \dots 18$ mm, when a magnetomotive force of $\hat{\Theta}_{bng} = 375$ At is applied. As stated before, the wider the tooth the larger are the passive reluctance forces, hence, the smaller is the radial starting distance that the active bearing can handle for a certain electrical excitation level. This relation is seen in the simulation results in **Fig. 9** as well. The achievable starting distance depends on the angular position of the rotor, i.e., how does a rotor magnet face the stator tooth. Therefore, **Fig. 9** not only depicts the average value for the starting distance (δ_{avg}) but also the minimum and maximum possible distances (δ_{min} and δ_{max}), representing the worst and best rotor positions for the active magnetic bearing. Additionally, these three parameters are plotted for the reference motor in grey. The results reveal that for a tooth width of 13 mm, the minimal starting distance δ_{min} coincides with the one of the reference motor. This implies that the three-pole motor's active magnetic bearing, can handle at least the same starting distance (i.e. to detach the rotor from the wall) as the reference motor for the same applied magnetomotive force. This direct comparison is possible, because the stator and rotor diameters have been set equal at the beginning of this study, i.e., have the same split ratio.

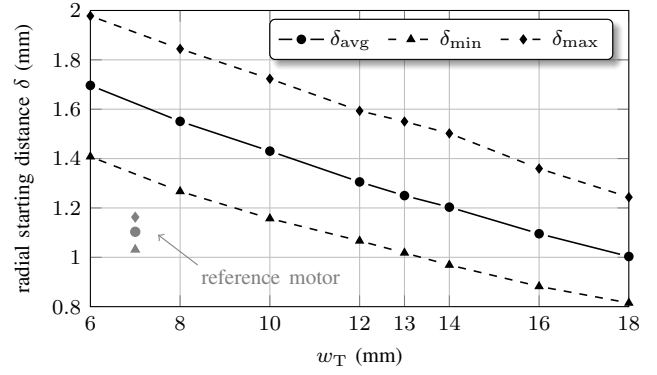


Fig. 9: Average (δ_{avg}), minimal (δ_{min}) and maximal (δ_{max}) possible starting distances of the novel three-pole motor (depending on rotor's angular position) for an electrical excitation of $\hat{\Theta}_{bng} = 375$ At with respect to different stator tooth widths w_T . Additionally, the average, minimal and maximal starting distances of the reference motor are marked in grey.

To sum up the coupled three-pole motor's investigation, a stator design with $w_T = 13$ mm and no tooth tip offers a high drive torque, rather low cogging torque and bearing forces, that are comparable to the reference motor's active magnetic bearing. The optimal design parameters, bearing and drive characteristics are listed in **Tab. II** and its magneto-static behavior obtained from 3D FEM simulations is depicted in **Fig. 10**. It should be noted that a brief analysis of the tilting and axial stiffnesses confirmed, that unlike for slice motors, these passive stabilities are not critical for double-sided driven shafts.

V. LOSSES

This section covers a brief comparison of the novel three-pole and the reference motor's losses. This is particularly interesting for the future prototype. Generally, the largest share of the motor losses are the copper and iron losses. The copper losses P_{Cu} are defined as

$$P_{Cu} = m \cdot R \cdot I_{rms}^2, \quad (7)$$

where m is the tooth number, R the copper resistance and I_{rms} the effective value of the phase current. The resistance

TABLE II: Optimal design parameters of the novel three-pole motor and its bearing and drive characteristics.

| Parameter | | | |
|--|---------------|------|-------|
| tooth tip opening angle | α_{TT} | — | deg |
| tooth tip thickness | t_{TT} | — | mm |
| tooth width | w_T | 13 | mm |
| drive torque constant (coupled) | k_{drv} | 0.35 | mNm/A |
| bearing force constant | k_{bng} | 26.9 | mN/A |
| radial stiffness | $c_{x,y}$ | 8.2 | N/mm |
| drive ripple factor for 250 At (coupled) | γ | 4.0 | % |

of the copper coils can further be calculated as

$$R = \rho_{\text{Cu}} \cdot \frac{l_{\text{coil}}}{A_{\text{wdg}}} \approx \rho_{\text{Cu}} \cdot \frac{l_{\text{wdg,avg}} \cdot N_{\text{coil}}^2}{A_{\text{coil}} \cdot k_{\text{coil}}}, \quad (8)$$

with the copper resistivity δ_{Cu} , slot filling factor k_{coil} , cross-sectional area of the coil A_{coil} , average winding length $l_{\text{wdg,avg}}$ and number of turns per coil N_{coil} . Furthermore, the phase current can be written as

$$I_{\text{rms}} = \frac{\hat{\Theta}/\sqrt{2}}{N_{\text{coil}}}, \quad (9)$$

where $\hat{\Theta}$ represents the magnetomotive force. Finally, plugging (8) and (9) into (7) and assuming the same slot filling factor k_{coil} for the three-pole motor as the reference motor has, following proportionality relation results

$$P_{\text{Cu}} \propto m \cdot \frac{l_{\text{wdg,avg}} \cdot \hat{\Theta}^2}{A_{\text{coil}}}. \quad (10)$$

The three-pole motor has a slot number of $m = 3$ (in contrast to the reference motor with $m_{\text{ref}} = 6$), much more space for bigger copper coils A_{coil} , however, a larger magnetomotive force $\hat{\Theta}$ is required to generate the same drive torque.

The stator iron is permeated by an oscillating magnetic field, so the field related hysteresis losses P_{hy} and eddy current losses P_{ed} make up the iron losses. P_{hy} per volume can be characterized as

$$P_{\text{hy}} = f(A_{\text{h}}, \omega) \quad (11)$$

where A_{h} represents the area enclosed by the hysteresis curve and ω the angular frequency of the field harmonic [10]. For P_{ed} per volume it holds that

$$P_{\text{ed}} = f(\sigma, B^2, \omega^2), \quad (12)$$

with σ being the electric conductivity and B the magnetic flux density [10]. A straight forward iron loss comparison for the three-pole and six-pole reference motor with relations (11) and (12) is not possible at this point. The motors have different frequencies of the harmonic field, different flux densities due to different stator geometries and the application specific operating point has not been defined yet.

After this brief loss discussion, it can be concluded that an operating point for the target application has to be defined followed by a detailed loss analysis and copper coil design. Only then, a direct comparison of the maximal achievable drive torque between the six-pole and coupled three-pole motors is reasonable. This in-depth analysis and the commissioning of a prototype will be the focus of future work.

VI. CONCLUSION

The novel three-pole bearingless motor has been introduced, which is particularly beneficial for double-sided driven applications. The motor combines an elegantly simple and minimalistic design (hardware-wise), while allowing a rotor operation in chemically challenging, high-purity or extreme temperature environments due to the hermetically-sealed encapsulation of the rotor. By means of 3D magnetostatic FEM simulations, the

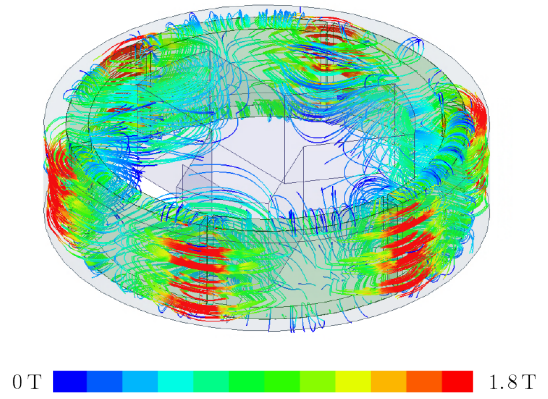


Fig. 10: Concept of the novel three-pole motor analyzed by 3D magnetostatic FEM simulations.

drive and bearing behavior of two coupled three-pole motors has been investigated and compared to a previously presented, fully operational reference motor. An optimal stator design has been found, which allows for a high drive torque with rather low cogging torque and sufficient bearing forces.

ACKNOWLEDGMENT

The authors gratefully thank the Swiss Innovation Agency Innosuisse for their financial support and Levitronix GmbH for their financial, scientific as well as technical contributions.

REFERENCES

- [1] S.-M. Yang, and M.-S. Huang, "Design and implementation of a magnetically levitated single-axis controlled axial blood pump," *IEEE Transactions on Industrial Electronics*, vol. 56, no. 6, pp. 2213-2219, Jun. 2009.
- [2] T. Reichert, T. Nussbaumer, and J. W. Kolar, "Bearingless 300-W PMSM for bioreactor mixing," *IEEE Transactions on Industry Applications*, vol. 59, no. 3, pp. 1376-1388, March 2012.
- [3] H. Sugimoto, I. Shimura, and A. Chiba, "Principle and test results of energy-saving effect of a single-drive bearingless motor in cooling fan applications," *IEEJ Journal of Industry Applications*, vol. 6, no. 6, pp. 456-462, 2017.
- [4] J. J. Ewing, "Excimer laser technology development," *IEEE Journal of selected topics in quantum electronics*, vol. 6, no. 6, pp. 1061-1071, 2000.
- [5] I. Bagaric, D. Steinert, F. Wassmer, T. Hostenstein, T. Nussbaumer, and J. W. Kolar, "Design and characterization of a bearingless cross-flow fan," in *2021 IEEE/ASME International Conference on Advanced Intelligent Mechatronics (AIM)*, Jul. 2021, pp. 1195-1200.
- [6] S. Earnshaw, "On the nature of the molecular forces which regulate the constitution of the luminiferous ether," *Transactions of the Cambridge Philosophical Society*, vol. 7, pp. 97-112, 1842.
- [7] F. Zürcher, T. Nussbaumer, and J. W. Kolar, "Principles of magnetic levitation and motor torque generation by superposition of harmonics in bearingless brushless motors," in *35th IEEE IECON*, Nov. 2009, pp. 1246-1251.
- [8] P. Karutz, T. Nussbaumer, W. Gruber, and J. W. Kolar, "Saturation effects in high acceleration bearingless motors," in *2008 IEEE International Symposium on Industrial Electronics*, June 2008, pp. 472-477.
- [9] T. Reichert, T. Nussbaumer, W. Gruber, and J. W. Kolar, "Design of a novel bearingless permanent magnet motor for bioreactor applications," in *2009 35th Annual Conference of IEEE Industrial Electronics*, Nov. 2009, pp. 1086-1091.
- [10] H. Mitterhofer, and W. Amrhein, "Design aspects and test results of a high speed bearingless drive," in *2011 IEEE Ninth International Conference on Power Electronics and Drive Systems*, Dec. 2011, pp. 705-710.